PNAS RESEARCH ARTICLE | CLASSIFICATION

Attention to heterogeneous information sources affects epidemic outcomes

Jiayu Li[a,b,1], Matthew Cheung[a,b], Marcela Ordorica Arango[c], Naomi Ehrich Leonard[c,1], and Simon A. Levin[b,d,1]

This manuscript was compiled on July 28, 2026

During an epidemic, disease transmission and human behavior are closely related: high infection levels trigger risk awareness and preventive behaviors, which suppress the transmission of disease. While these coupled dynamics have been heavily investigated, both in well-mixed populations and networked populations, less has been done to explore how different ways to establish the awareness of disease affect infection levels. This study presents a mathematical model of two interacting groups (populations) to investigate how epidemic outcomes are affected by the choice of information source, i.e., one's own group and/or the other group. We demonstrate that for different physical contact patterns the system can undergo a bifurcation from a uniform endemic equilibrium (UEE) to a non-uniform endemic equilibrium (NUEE), resulting in a persistent infection level difference between groups that is driven by each group's choice of its information source. Our results reveal strategies to minimize infection: 1) a group with low infection level benefits by prioritizing information from a group with high infection level thereby overestimating risk and 2) a group with high infection level benefits by accessing information only about its own infection level thereby avoiding underestimation of risk. These results emphasize the need to promote awareness of disease levels in addition to observation of anti-epidemic measures. We highlight conditions under which strategies that benefit one group may conflict with strategies that benefit the total infection level of both groups.

Infectious disease | Opinion dynamics | Dynamical system

Significance

The integration of human behavior into infectious disease models has been investigated a lot, and it is well-recognized that human behavior drastically affect the epidemic outcome. However, less has been done to learn how different information sources for perceived infection levels affect the coupled behavior-disease dynamics. We propose a simple model that focuses on how attention to heterogeneous information sources when evaluating the risk of disease affects the epidemic outcomes. Our findings suggest that the choice of information source can lead to variations in epidemic sizes across different populations, informing informational strategies that help to minimize infection levels. The findings may offer insights for policy makers regarding the role of reporting infection levels from other regions.

People's changing behaviors and the spread of infectious disease are not isolated processes. Different behavioral patterns, including willingness to wear masks, get vaccinated, and observe social distancing, can suppress the transmission of disease (1). Meanwhile, the spread of disease may in turn influence people's behaviors by altering risk perception (2). For instance, the demand for condoms increased in areas where AIDS was prevalent (3). More recently, people engaged in social distancing and hygiene behaviors even at the onset of the COVID-19 pandemic (4). However, as those preventive behaviors hindered the spread of disease, awareness of disease levels waned. Even though COVID-19 still spreads (5), less effort is put on reporting the daily cases (6) and mask mandates have been removed in most countries (7).

The importance of integrating human behavior into infectious disease models has been well-established in the past decades. Ref. (8) shows that, even without knowledge-based adaptation of human behavior (i.e., behavior not coupled with knowledge of disease transmission), heterogeneity in the social activity level of individuals still affects the epidemic outcome. For the coupled behavior and disease dynamics, systematic reviews (9–12) investigate a broad range of infectious disease, including AIDS, influenza, Zika, Ebola, and COVID-19, and human behaviors, including getting vaccinated and observing social distancing. As many of the models consider a well-mixed population (13–15), where there is no spatial or contact pattern in the population structure, a growing number of studies have started to incorporate population structure and heterogeneity into models of information and disease transmission (1, 16–22). These considerations are essential as infectious disease can only spread through physical contact or close proximity with infected individuals (given airborne propagules) and awareness of disease can be established through

Author affiliations: [a]Program in Applied & Computational Mathematics, Princeton University, Princeton, NJ 08540, USA; [b]High Meadows Environmental Institute, Princeton University, Princeton, NJ 08540, USA; [c]Department of Mechanical and Aerospace Engineering, Princeton University, Princeton, NJ 08540, USA; [d]Department of Ecology and Evolutionary Biology, Princeton University, Princeton, NJ 08540, USA

Jiayu Li, Naomi Ehrich Leonard, Simon A. Levin designed research; Jiayu Li performed research; Naomi Ehrich Leonard, Simon A. Levin supervised research; Jiayu Li, Matthew Cheung, Marcela Ordorica Arango, Naomi Ehrich Leonard, Simon A. Levin wrote the paper.

The authors declare no conflict of interest.

[1]To whom correspondence should be addressed. E-mail: jl2894@princeton.edu, naomi@princeton.edu, slevin@princeton.edu

face-to-face conversation, phone calls with friends, and mass media (23). While the spread of infectious disease is constrained by physical distance, information on the infection levels can travel across the globe quickly. For instance, over 7000 articles regarding COVID from major press media were published within a month of the initial outbreak in China (24), although only around 1200 confirmed cases outside China were reported at that time (25). People around the world became aware of the disease even when there might not have been infections around them. One important contribution that addresses this scale mismatch between disease and information transmission is made by Funk et.al (1), where they find that even without global information about the infection level, the behavioral response at the local level through a social network may prevent the disease from spreading. Continuing along this line, several studies treat the coupled dynamics as a spatially heterogeneous process and investigate them in networked populations (17, 18). Other studies focus on integrating behavioral components into epidemic models under reaction–diffusion partial differential equation settings, where individuals that perceive high risk through spatial information (local, non-local or global) reduce their mobility (19–21). Further studies treat the information spread as a dynamic process and explore the effect of population structure on specific behavioral patterns that affect disease transmission, such as vaccine hesitancy (21) and homophily in attitude towards vaccination (22).

Our study contributes to the literature by incorporating the heterogeneity of information source into coupled disease-opinion dynamics. To the best of our knowledge, previous models restrict to a prescribed information source for risk perception, while the effect of different choices of information source remains less understood. People have access to information about both local infection levels and infection levels from other regions (26). Consequently, people have a choice when establishing their assessment of risk of disease, which guides their behavioral changes: they can focus on the infection level within their own community, on reports from (potentially) distant communities or on some combination of both. Studies have shown that people's perceived disease risk may not align perfectly with local information (27). Sometimes, closer distance to an epicenter may be associated with lower risk perception of the pandemic (28). Another study shows that people tend to underestimate the local pandemic risk compared to the rest of the world. Such spatial optimism might emerge from psychological distancing mechanisms where remote threats are perceived to be more serious, while local threats are downplayed (29). As empirical and quantitative evidence of how exactly people perceive infection risk based on local infection level versus infection level from another region is still scarce, our study aims to provide some theoretical insight on how people's choice of information source when evaluating the risk of the disease affects the epidemic outcome.

To investigate this question, we introduce a two-population mathematical model of the coupled disease and awareness dynamics extended from (15). The two populations represent two interacting groups* of people with physical and informational interactions, such that each of the two types of interactions can happen within groups and between groups, potentially at different frequencies. For disease transmission, we consider the Susceptible-Infected-Recovered-Susceptible (SIRS) dynamics (30), with an effective infection rate that changes with behavior implied by changing perceived infection level. For analytical tractability, in the main text, we present the special case where the rate of waning immunity of the disease goes to infinity, i.e., the disease transmission follows the Susceptible-Infected-Susceptible (SIS) dynamics. The relevant numerical results for the more general SIRS case are included in the Supplemental Information. We investigate when the system transitions from an infection free equilibrium (IFE) to a uniform endemic equilibrium (UEE), where the two groups have the same infection levels. We show how the choice of information source may lead to a non-uniform endemic equilibrium (NUEE), where the two groups end up with different infection levels. We use this framework to determine the optimal information choice that minimizes a group's own infection level, and we explore the implications of this choice for prosocial outcomes.

Our analysis reveals how attention to heterogeneous information sources affects the epidemic outcomes: a group with low initial infection level may minimize its infection by mainly considering the infection level of a more highly infected group. This other group acts as a cautionary tale and promotes higher vigilance of the disease transmission. A group with an initially high infection level should focus its attention on its own infection level to avoid underestimating risk, which may happen if it attends to a group with a lower infection level. We also show that incentives to minimize infection level within one's own group may conflict with prosocial goals across the two groups.

Materials and Methods

Mathematical Model. We introduce the model studied in the main text with illustration in Fig. 1A. The disease transmission follows SIS dynamics, while each group's effective infection rate is affected by its perception of the epidemic risk, determined by its information source. See below for a detailed derivation of the model.

We note that it is not necessary to assume SIS dynamics of disease transmission. For the more general case in which the disease transmission follows the Susceptible-Infected-Recovered-Susceptible (SIRS) dynamics (30), where infected individuals gain temporary immunity to the disease, most of the results presented hold as long as the rate of waning immunity is sufficiently high. In the main text, for analytical tractability, we use SIS dynamics as a limiting case for SIRS, where immunity disappears immediately after recovery. In the Supplemental Information, we present numerical results for the general case of SIRS.

First, consider a disease spread in a well-mixed population, following the standard SIS dynamics (30). Let $p(t), s(t)$ denote the fraction of infected and susceptible individuals in the population, respectively. Susceptible individuals get infected with rate $\beta\ (day^{-1})$ through physical interaction with infected individuals, and infected individuals recover with rate $\delta\ (day^{-1})$. The dynamics can be described by

$$\frac{ds}{dt} = -\beta sp + \delta p, \quad \frac{dp}{dt} = \beta sp - \delta p$$

Since $s(t) = 1 - p(t)$, the SIS dynamics can be reduced to the single equation

$$\frac{dp}{dt} = \beta p(1-p) - \delta p.$$

Lajmanovich and Yorke (31) extend the model to consider heterogeneity in population structure. For the purpose of our model, we adapt (15, 31) into a two-population model, where the effective physical contact rate within

*In this paper, we use 'population' and 'group' interchangeably.

each subpopulation is denoted by $k \in [0,1]$ (unitless), and the effective physical contact rate between the two subpopulations is denoted by $1-k$:

$$\frac{dp_1}{dt} = \beta(kp_1 + (1-k)p_2)(1-p_1) - \delta p_1$$
$$\frac{dp_2}{dt} = \beta(kp_2 + (1-k)p_1)(1-p_2) - \delta p_2.$$

To incorporate human behavior into this two-population model, we introduce into the dynamics the perceived infection level p_{si} of each group i, $i = 1, 2$. There is evidence that high perceived infection level leads to more preventive behaviors during disease transmission (27, 32). We incorporate this effect by considering the effective infection rate $\beta\alpha(p_{si})$ of group i, which decreases with increasing perceived infection level p_{si}. That is, higher perceived infection level triggers more preventive behaviors, which reduces the effective infection rate of the transmission of the disease. Although the theoretical proof does not depend on the specific form $\alpha(\cdot)$, given $\alpha(\cdot)$ is a decreasing function with range $[0,1]$, we assume people adopt behavioral change according to a soft-threshold (33) with $\alpha(\cdot)$ taking the following form (15) (Fig 1B):

$$\alpha(p_s) = \begin{cases} 1 - \frac{1}{1+\left(\frac{p_s(1-\mu)}{\mu(1-p_s)}\right)^{-\nu}} & \text{if } p_s \in (0,1] \\ 1 & \text{if } p_s = 0 \end{cases}$$

where $\mu \in (0,1)$ controls the threshold above which the perceived infection level triggers behavioral response, and $\nu \in (0,\infty)$ determines the abruptness of the response. The greater is ν, the more abruptly $\alpha(\cdot)$ decreases around μ.

We let the dynamics of the perceived infection level p_{si} depend linearly on the actual infection level, represented as $\eta_i p_i + (1-\eta_i)p_j$ where $\eta_i \in [0,1]$ is group i's choice of information source. This representation of actual infection level is a form of "information variable (index)" discussed in (13, 14). Larger η_i means group i focuses more on the infection level within group i when evaluating the risk of disease. This gives dynamics of the form

$$\tau\frac{dp_{si}}{dt} = -p_{si} + \eta_i p_i + (1-\eta_i)p_j, \quad j \neq i,$$

where τ (day) accounts for relative time scale of awareness establishment compared to the disease spread. See the Supplemental Information for the derivation. Larger τ means it takes more time for people to update the perception of disease based on the information they receive.

Combining all of these pieces together, we arrive at a 4-dimensional system that we investigate in this paper:

$$\begin{aligned} \frac{dp_1}{dt} &= \beta\alpha(p_{s1})(kp_1 + (1-k)p_2)(1-p_1) - \delta p_1 \\ \frac{dp_2}{dt} &= \beta\alpha(p_{s2})(kp_2 + (1-k)p_1)(1-p_2) - \delta p_2 \\ \tau\frac{dp_{s1}}{dt} &= -p_{s1} + \eta_1 p_1 + (1-\eta_1)p_2 \\ \tau\frac{dp_{s2}}{dt} &= -p_{s2} + \eta_2 p_2 + (1-\eta_2)p_1. \end{aligned} \quad [1]$$

For simplicity, we rescale the system so that $\delta = 1$. We also let $\tau = 1$ as τ does not affect the values and stability of the equilibria we study, nor the type of local bifurcations of our study. We retain a positive value of τ since the assumption $\tau = 0$, i.e., instantaneous update in perception of infection levels, is impractical and $\tau > 0$ does affect the transient dynamics of the system. See the Supplemental Information for the proof and more discussion.

With this model we are able to study, for different β, k and $\alpha(\cdot)$, how the choices of η_1 and η_2 affect the equilibrium infection levels of group 1 and group 2, as well as the infection level of the total population (group 1 plus group 2).

Stability and Bifurcation Analysis. We perform linear stability analysis (34) of the equilibria of interest to determine the parameter values where there is a change in stability of the equilibria.

The bifurcation point is determined when the largest real part of the eigenvalues of the Jacobian matrix at equilibrium crosses zero. To determine the type of bifurcation, we perform Lyapunov Schmidt reduction (35, 36), which is a low-dimensional reduction of the system that describes the local topology around the bifurcation point. In particular, this technique allows us to reduce the local bifurcation diagram for the system to the one-dimensional equation: $f(x,\gamma) = c_1\gamma + c_2\gamma x + c_3 x^2 + c_4 x^3 + h.o.t. = 0$, where x is a scalar that describes the restriction of the dynamics along the tangent to the bifurcation manifold, γ is the shifted bifurcation parameter, and both are assumed small in magnitude. The signs of c_1, c_2, c_3, c_4 determine the local topology near the bifurcation. Sometimes those coefficients can be determined analytically. For the closed-form expressions that are hard to obtain, the coefficients are computed numerically in Mathematica (37). We use MatCont (38) to generate bifurcation diagrams.

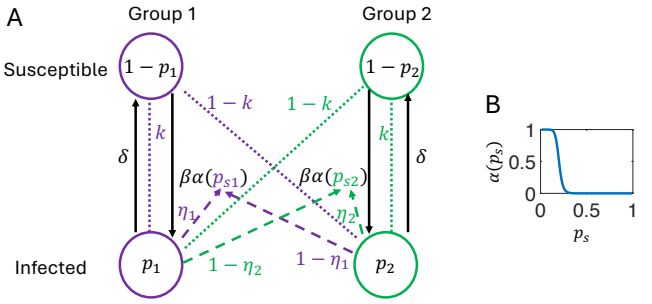

Fig. 1. Panel A: illustration of the model setup. Solid black line represents the connection between susceptible compartments and infected compartments. Purple denotes group 1 and green denotes group 2. Dashed line represents source of information for perceived risk of disease, arrow points from the source of information to the affected group perception. Dotted line represents the physical interaction between susceptible individuals with infected individuals (from both groups). Panel B: an example of $\alpha(\cdot)$ used in the numerical simulation, $\mu = 0.2, \nu = 8$.

Numerical Simulation. We use ode45 in MATLAB (39) to simulate the dynamics of the system for different parameter values and initial conditions.

To explore how the choice of η_i affects the epidemic outcome, we consider 100 evenly spaced values of η_1 and 100 of η_2 in $[0,1]$. For each pair of (η_1, η_2) values, we consider two cases: $p_1(0) > p_2(0)$ and $p_1(0) < p_2(0)$, with $p_{s1}(0) = \eta_1 p_1(0) + (1-\eta_1)p_2(0), p_{s2}(0) = \eta_2 p_2(0) + (1-\eta_2)p_1(0)$. $p_i(0)$s are sampled randomly from a uniform distribution for each simulation. The dynamics are run until the system reaches equilibrium, and the equilibrium values of p_1 and p_2 are recorded for further analysis. See figure captions for the parameter values chosen.

Information source does not affect the establishment of disease in the total population.

It is well known that, in the classical SIS model in a well-mixed population, if the basic reproduction ratio $\mathcal{R}_0 = \frac{\beta}{\delta} > 1$, the disease persists (40). A comparable result for our model is shown, where since $\delta = 1$ and $\alpha(0) = 1$, if $\frac{\beta}{\delta} = \beta > \frac{1}{\alpha(0)} = 1$, the disease will persist in at least one of the groups.

The system undergoes a transcritical bifurcation at $\beta = 1$, where the infection-free equilibrium (IFE, $p_1 = p_2 = p_{s1} = p_{s2} = 0$) and the uniform endemic equilibrium (UEE, $p_1 = p_2 = p_{s1} = p_{s2} = p$) exchange stability (Fig 2A). See the Supplemental Information for the proof.

This bifurcation point only depends on the value of β. As a result, the physical contact pattern and the information exchange pattern do not affect the establishment of the disease in the whole population, which is also shown in previous literature (15, 17). There is no choice of k and η_i that can eliminate the disease from the total population once $\beta > 1$. However, as we show, the choice of information source, i.e., choice of η_i, may help one of the two groups get rid of the disease even when $\beta > 1$.

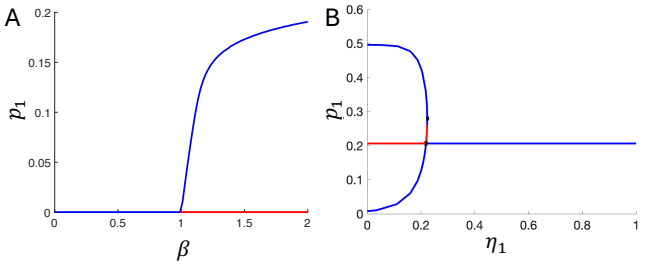

Fig. 2. Bifurcation diagrams plot equilibrium values of p_1 (stable in blue and unstable in red) as a function of a bifurcation parameter β (Panel A) and η_1 (Panel B). A: When $\beta = 1$, the system undergoes a transcritical bifurcation from IFE to UEE. $k = \eta_1 = \eta_2 = 0.6$, $\nu = 8$, $\mu = 0.2$. B: When $\eta_1 = \eta^*$, the system undergoes an unfolding of a pitchfork bifurcation which locally exhibits as a transcritical bifurcation from UEE to NUEE. $\beta = 3$, $k = \eta_2 = 0.6$, $\nu = 8$, $\mu = 0.2$.

Two groups may end up with different infection levels due to the choice of information source.

Assuming $\beta > 1$, mathematical analysis (see details in the supplemental information) shows that the UEE is asymptotically stable if the choices of information source satisfy

$$\eta_1 + \eta_2 > \frac{1 - 2k + \beta\alpha(p)}{\beta\alpha'(p)p(1-p)} + 1 = C_0. \qquad [2]$$

Since p at the UEE is defined by $\beta\alpha(p)(1-p) = 1$, the infection level at the UEE is not affected by the information source.

Without loss of generality (as the system is symmetric with respect to η_1 and η_2), let η_1 be the bifurcation parameter. When $\eta_1 < \eta^* = C_0 - \eta_2$, the UEE loses stability. The system contains an unfolding of a pitchfork bifurcation, where it undergoes a transcritical bifurcation locally at $\eta_1 = \eta^*$ (Fig. 2B). See the Supplemental Information for the proof. We call the new stable equilibrium a non-uniform endemic equilibrium (NUEE), since the two groups have different equilibrium infection levels.

Although the different equilibrium infection levels were observed in previous work (17), the reason for that was not made clear. Here, we show that such a difference in infection levels is driven by the information contact pattern (η_i) instead of the physical contact pattern (k).

From Eq. **2**, since $\alpha'(\cdot) < 0$, η^* increases as k and β increase and η_2 decreases.

The UEE stability condition Eq. **2** has two implications (see the supplemental information for detailed analysis):

1. Regardless of $\alpha(\cdot)$, β and k, if $\eta_1 + \eta_2 \geq 1$, the UEE is always stable. This means that

   a) For the system to enter the NUEE regime, at least one group needs to prioritize the information from the other group for risk evaluation (i.e., at least one of η_is needs to be less than $\frac{1}{2}$). This can happen, e.g., if there is no official report of the infection data in one group (41, 42), or people do not trust the infection level reported from their own population (43).

   b) If each group i only cares about the infection within group i, i.e., $\eta_i = 1$, then the two groups will have the same equilibrium infection levels.

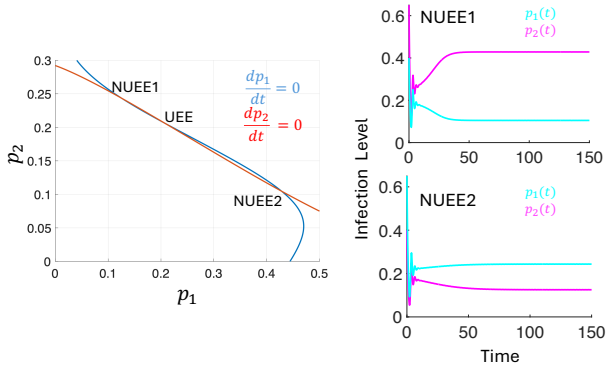

Fig. 3. Left: the projection of the nullclines (where the rate of change of the variable is 0) on the (p_1, p_2) plane. Intersections of the nullclines suggest the exsitence of two NUEE in the (p_1, p_2) plane. Right: Depending on the initial conditions, the system ends up at different equilibrium infection levels. $\beta = 3$, $\eta_1 = 0.2$, $k = \eta_2 = 0.6$, $\nu = 8$, $\mu = 0.2$.

2. Regardless of η_1, η_2 and k, β needs to be strictly greater than 1 for the UEE to lose stability. Moreover, there is no direct transition from IFE to NUEE.

Note that if the disease transmission follows SIRS dynamics, numerically, the choice of information source can still lead to the different equilibrium infection levels of the two groups, given that the rate of waning immunity is high enough. See the Supplemental Information, in particular Fig. S6A and Fig. S6B for more details. When the rate of waning immunity is lower, on the other hand, the information source affects the transient dynamics of the system (Fig. S7), but not the equilibrium.

Choice of information source may increase or decrease the epidemic size within group.

As the bifurcation from UEE to NUEE is an unfolding of a pitchfork bifurcation, two NUEE equilibria exist (Fig. 3): either $p_1 < p_2$ (NUEE1) or $p_1 > p_2$ (NUEE2). Which equilibrium the system ends up with depends on the initial conditions. Those two equilibria are not symmetric, i.e., the equilibrium value of p_1 at NUEE1 is not the same as the equilibrium value of p_2 at NUEE2.

Suppose the groups' perceived infection levels at the beginning follow their information source, i.e.,

$$\begin{aligned} p_{s1}(0) &= \eta_1 p_1(0) + (1-\eta_1)p_2(0) \\ p_{s2}(0) &= \eta_2 p_2(0) + (1-\eta_2)p_1(0). \end{aligned} \qquad [3]$$

Then $p_1(t) \leq p_2(t)$ if $p_1(0) < p_2(0)$. See the Supplemental Information for the proof.

This means that, within the NUEE regime, the group that starts with lower infection level will end up with lower infection level compared to the infection levels of both the UEE and the group that starts with higher infection level. Conversely, the group that starts with the higher infection level will end up with a higher infection level compared to the infection level of both the UEE and the group that starts with the lower infection level, see Fig 4.

Thus, the NUEE regime is beneficial for the group that starts with a lower infection level, while the UEE regime is better for the group that starts with a higher infection level. Here we consider group 1 as the focal group. Based on the discussion in the previous section, if group 1 starts

with the lower infection level and $\eta_1 = 0$, i.e., group 1 prioritizes the infection level of group 2 for risk assessment, the system is more likely to end up in an NUEE region, which is optimal for minimizing group 1's equilibrium infection level. Notice that if group 1 starts with the higher infection level, such focus on the other group may lead to a higher equilibrium infection level. However, if $\eta_1 = 1$ in this case, i.e., group 1 only takes into account the within-group infection, the system will end up in the UEE region, which minimizes the final epidemic size of group 1. In summary, the optimal informational strategy to minimize group-level infection is to focus on the infection level of the group that starts with higher infection when evaluating the risk of disease. This optimal informational strategy is still valid when the disease transmission follows SIRS dynamics. For high rate of waning immunity, the equilibrium infection level of the group can be minimized, see Fig. S6C. For low rate of waning immunity, even when the bifurcation from UEE to NUEE does not happen, a group is better off if it focuses its source of information on the group with the higher initial infection level, in the sense that the peak infection level of the group during the first wave of epidemic is lower, see Fig. S7B.

A direct consequence of the optimal strategy is that if both groups follow it strictly, then the system will be in the UEE regime. The group that starts with the higher infection level only cares about the within-group infection, i.e., it chooses $\eta_i = 1$. According to our analysis, if $\eta_i = 1$ for either group, the system will end up in the UEE regime.

Although the optimal strategy only involves the choice of η_i, and is unaffected by different values of the within-group physical contact rate k, as discussed above, a smaller k means a smaller NUEE region in the (η_1, η_2) plane. Furthermore, k affects the actual equilibrium infection level at NUEE (Fig. 4). As the within-group physical interaction becomes more frequent (increasing k), the final endemic sizes for the two groups are more different. More frequent between-group physical contact (decreasing k) ensures more frequent exchange of infection cases between the two groups, making it harder for the two groups to have different infection levels.

For large k values that are close to 1, it is possible for the final epidemic size within a group to be zero (Fig. 4, bottom right plot). When the group starts with lower infection refers to the infection level of the other group, it overestimates the risk and "over-reacts" by observing stricter anti-epidemic measures, which reduces the actual epidemic size within the group. If most of the physical interactions happen within the group, such overestimation is strong enough to eliminate the disease transmission within the group.

There is evidence that people's awareness of disease is largely affected by media reporting (44, 45). The information source in this study can be considered as what is reported by the media. For a focal group having an ill-behaved neighboring group, massively reporting the high infection levels in that group may help to contain the spread of disease within the focal group. For instance, by January 30, 2020, over 9000 cases of COVID across the globe were reported, while only one case in the U.S. was confirmed (46). The awareness established from the reported infection levels in these other countries helped the U.S. to contain the local spread of COVID-19 by encouraging multiple preventive behaviors, including

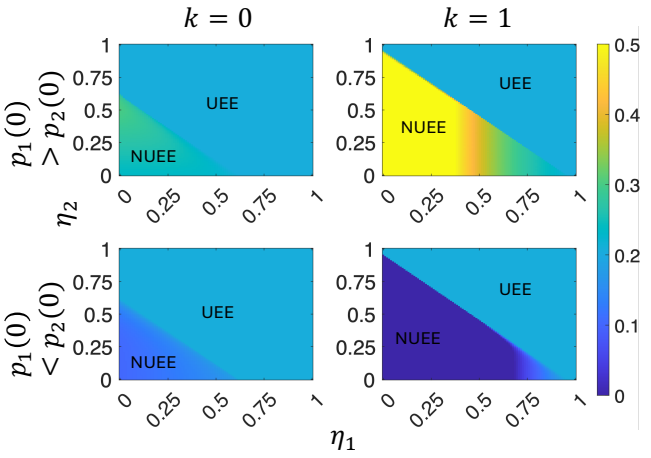

Fig. 4. The equilibrium infection level p_1 (color scale) for different initial conditions and values of k, η_1 and η_2. Regardless of the value of k, if $p_1(0) > p_2(0)$, the system will end up at NUEE2 (upper panel). If $p_1(0) < p_2(0)$, the system will end up at NUEE1 (lower panel). In each subplot, top right region is the region for UEE, and bottom left is the region for NUEE. Higher k corresponds to larger NUEE region in (η_1, η_2) plane and greater difference between the infection levels at NUEE and UEE. When k is large and $p_1(0) < p_2(0)$, the equilibrium infection in group 1 can be 0. $\beta = 3, \mu = 0.2, \nu = 8$.

screening passengers at certain airports (47). Less than 100 cases in the U.S. were reported in February 2020 (48).

More generally, at the early stage of disease transmission, the awareness in one group of the disease established in another group with a high level of infection allows people within the focal group to take action sooner than they would if they only referred to their own infection levels. If the physical interaction with the other group is infrequent enough, it is possible for the focal group to get rid of the disease completely. This inspires an interesting question: can media emphasize the severity of an infectious disease by mainly reporting cases in the region with highest epidemic size to trigger people's cautious reaction? While there is a large literature that focuses on the misinformation of epidemic spread by the media (49, 50), the effect of different emphasis of media reporting is less well understood, and could be interesting for future study.

The group-wise optimal information choice conflicts with pro-social goals.

Sometimes, a group might be prosocial: in addition to caring about the infection level within their own group, people may also try to minimize the infection level in the other group. Consider group 1 and suppose that instead of minimizing p_1, people seek to minimize $(1-\gamma)p_1 + \gamma p_2$, $\gamma \in [0, \frac{1}{2}]$, at equilibrium, where γ is a prosocial coefficient that accounts for how much group 1 cares about group 2 compared to themselves. $\gamma = 0$ corresponds to the case where group 1 does not care about group 2 at all, and $\gamma = \frac{1}{2}$ corresponds to the case where group 1 cares about the two groups equally.

For $p_1(0) < p_2(0)$, since we know that $p_1(t) \le p_2(t)$, it is enough to check $\gamma = \frac{1}{2}$, which is included in Fig. 5. The more interesting case is when $p_1(0) > p_2(0)$. Our previous results suggest that p_1 at equilibrium is minimized in the UEE region, where $\eta_1 = 1$ is the optimal choice. Numerical simulations show, for some $\gamma < \frac{1}{2}$, that $(1 -$

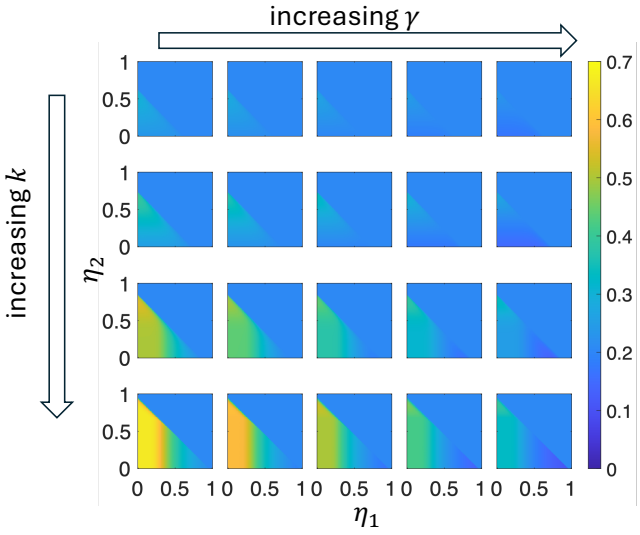

Fig. 5. The equilibrium infection level $(1-\gamma)p_1+\gamma p_2$ in color scale for different values of k and γ when $p_1(0) > p_2(0)$. $\beta = 3$, $\mu = 0.2$, $\nu = 8$.

$\gamma)p_1+\gamma p_2$ is minimized in the NUEE region (the bottom left triangle in each square of Fig. 5). This implies that the informational strategy for the prosocial goal is different from the optimal informational strategy to minimize the within-group infection level. When $\gamma = \frac{1}{2}$, i.e., when group 1 seeks to minimize (p_1+p_2), the final epidemic size in at least one group will be higher than if group 1 only cares about its within-group infection level.

We can see that $\frac{1}{2}(p_1+p_2)$ at equilibrium (the last column in Fig. 5) is both minimized and maximized in the NUEE region. The strategy that minimizes p_1+p_2 involves an optimal choice of both η_1 and η_2, i.e., choices by groups 1 and 2. Suppose group 1 starts with a higher infection level, then choices of $\eta_2 = 0$ and η_1 large enough but still less than C_0 will minimize p_1+p_2. However, a smaller η_1 and larger η_2 will result in higher p_1+p_2 at equilibrium in the NUEE region than that in the UEE region.

We note that the total infection level p_1+p_2 at the UEE is higher than that at certain NUEE. This is not very intuitive: it suggests that having a group that consistently behaves slightly worse compared to the other group is good for the total population, regardless of the physical contact pattern. In this scenario, although the group with higher infection level mainly focuses on the within-group infection, it still pays some attention to the information from the other group. This slight underestimation of the risk leads to slightly higher within-group infection level compared to the UEE, but this helps the total population because it is enough to trigger vigilance in the other group to stay cautionary. This effect could be further explored by considering groups of different sizes.

For the more general SIRS dynamics of the disease transmission, the mismatch between the optimal informational strategy for one group and the optimal informational strategy for the whole population still exists, given the rate of waning immunity is sufficiently high (Fig. S6D).

Conclusions and Future Directions

In this paper, we investigate how the information source used to evaluate the risk of disease affects the infectious disease dynamics. We develop a mathematical model extended from (15) to represent the physical and informational interactions between two groups during an epidemic. We find that, although the choice of information source does not affect the establishment of disease in the whole population, it can be a driver for different equilibrium infection levels within the two groups. In particular, a group can benefit from only referring to data on the group that has the higher infection level, regardless of the physical contact pattern. If the physical interaction between groups is not frequent, with this strategy the group that starts with lower infection can eventually reach an infection-free state, even when the infection rate is high.

However, such a strategy contradicts a strategy intended to minimize the total infection level of the two groups. We demonstrate that the within-group optimal informational strategy, i.e., always referring to the higher infection level of the two groups, does not help to minimize the total epidemic size of the two groups.

In the main text, we present the model where the disease transmission follows SIS dynamics for analytical tractability. As infections with coronaviruses, human parainfluenza viruses, respiratory syncytial viruses usually result in short-term immunities that decline over time (51), SIRS-type of disease transmission is more realistic for modeling those. Numerically, we show in our Supplemental Information that most of the results present in the main text hold when the disease transmission follows the more general SIRS dynamics, assuming that the rate of waning immunity is sufficiently high—this includes the transcritical bifurcation with respect to the information choice and the optimal informational strategy for the group and for the whole population. This makes sense intuitively because if the immunity wanes quickly enough, i.e., the reinfection happens soon after the previous infection, the disease can be approximated by SIS dynamics. On the other hand, if the immunity persists over the long term, the information source affects the transient dynamics, but not the equilibrium of the epidemic. Under this regime, the SIRS dynamics result in very low infection level among waves of epidemics, as they present more features of Susceptible-Infected-Recovered (SIR) dynamics (without demographics), which have zero infection level at equilibrium (30). The low infection level among waves of high infections cannot trigger sustained vigilance that would alter the equilibrium. We leave to future work more accurate parametrization of the model to fit a specific disease like SARS as well as the analytical study of our model with SIRS dynamics.

Other interesting factors can be added to the model to make it more realistic. For instance, instead of two groups of people, multiple groups may generate richer behavior. Another natural extension is to allow η_i to change over time. Our model assumes faithful and instant reporting of the infection levels of the two groups. Interactions between misinformation or delay (52) and the information source are worth exploring, i.e., what if the infection level reported about one group is inaccurate or outdated? The current setting also has no negative effects for overestimation of the disease, where

people can follow the strictest anti-epidemic measures without any negative consequences. However, an overly strict measure can negatively affect economic productivity and people's mental health (53, 54), while it may not always lead to significant decrease in infection counts (55). In the Supplemental Information, we report some preliminary results on how the constant negative effect of overestimation affects the epidemic outcomes. To better understand the phenomenon, in future work, we plan to add a feedback term to $\alpha(\cdot)$, potentially from an evolutionary game theory perspective (56), where the economic or psychological factors dynamically affect people's response to perceived infection.

Data, Materials, and Software Availability. Code used for this manuscript is available at https://github.com/jyl17/information_disease_interaction.

ACKNOWLEDGMENTS. J.L., M.C., and S.A.L. acknowledge a gift from William H. Miller III. J.L., M.C., and S.A.L. further acknowledge support from National Science Foundation- DMS-2327711- Collaborative Research: IHBEM: Data-driven multimodal methods for behavior-based epidemiological modeling. M.O.A. and N.E.L. acknowledge support from Air Force Office of Scientific Research grant FA9550-24-1-0002. N.E.L. and S.A.L. acknowledge support from the Army Research Office under Grant Number W911NF2410126. The views and conclusions contained in this document are those of the authors and should not be interpreted as representing the official policies, either expressed or implied, of the Army Research Office or the U.S. Government. The U.S. Government is authorized to reproduce and distribute reprints for Government purposes notwithstanding any copyright notation herein.

1. S Funk, E Gilad, C Watkins, VA Jansen, The spread of awareness and its impact on epidemic outbreaks. *Proc. Natl. Acad. Sci.* **106**, 6872–6877 (2009).
2. Z Wang, MA Andrews, ZX Wu, L Wang, CT Bauch, Coupled disease–behavior dynamics on complex networks: A review. *Phys. Life Rev.* **15**, 1–29 (2015).
3. A Ahituv, VJ Hotz, T Philipson, The responsiveness of the demand for condoms to the local prevalence of AIDS. *J. Hum. Resour.* pp. 869–897 (1996).
4. TR Fetzer, et al., Global behaviors and perceptions at the onset of the COVID-19 pandemic, (National Bureau of Economic Research), Working Paper 27082. DOI: 10.3386/w27082 (2020).
5. COVID-19 surveillance data in the United States (https://www.cdc.gov/covid/php/surveillance/index.html) (2025) Accessed: 2025-10-08.
6. Johns Hopkins COVID-19 data hub ends after three years (https://hub.jhu.edu/2023/03/10/coronavirus-resource-center-data-hub-ends/) (2023) Accessed: 2025-10-08.
7. R Mehra, B Patterson, P Riley, T Planche, A Breathnach, Impact of removing the healthcare mask mandate on hospital-acquired COVID-19 rates. *J. Hosp. Infect.* **145**, 59–64 (2024).
8. AV Tkachenko, et al., Stochastic social behavior coupled to COVID-19 dynamics leads to waves, plateaus, and an endemic state. *Elife* **10**, e68341 (2021).
9. P Manfredi, A D'Onofrio, *Modeling the interplay between human behavior and the spread of infectious diseases.* (Springer Science & Business Media), (2013).
10. J Bedson, et al., A review and agenda for integrated disease models including social and behavioural factors. *Nat. Hum. Behav.* **5**, 834–846 (2021).
11. F Verelst, L Willem, P Beutels, Behavioural change models for infectious disease transmission: a systematic review (2010–2015). *J. The Royal Soc. Interface* **13** (2016).
12. Z Wang, et al., Statistical physics of vaccination. *Phys. Reports* **664**, 1–113 (2016).
13. A d'Onofrio, P Manfredi, E Salinelli, Vaccinating behaviour, information, and the dynamics of SIR vaccine preventable diseases. *Theor. population biology* **71**, 301–317 (2007).
14. A d'Onofrio, P Manfredi, Information-related changes in contact patterns may trigger oscillations in the endemic prevalence of infectious diseases. *J. Theor. Biol.* **256**, 473–478 (2009).
15. Y Zhou, SA Levin, NE Leonard, Active control and sustained oscillations in actsis epidemic dynamics. *IFAC-PapersOnLine* **53**, 807–812 (2020).
16. AV Tkachenko, et al., Time-dependent heterogeneity leads to transient suppression of the COVID-19 epidemic, not herd immunity. *Proc. Natl. Acad. Sci.* **118**, e2015972118 (2021).
17. A Bizyaeva, MO Arango, Y Zhou, S Levin, NE Leonard, Active risk aversion in SIS epidemics on networks in *2024 American Control Conference (ACC)*. (IEEE), pp. 4428–4433 (2024).
18. K Peng, et al., A multilayer network model of the coevolution of the spread of a disease and competing opinions. *Math. Model. Methods Appl. Sci.* **31**, 2455–2494 (2021).
19. A d'Onofrio, M Banerjee, P Manfredi, Spatial behavioural responses to the spread of an infectious disease can suppress Turing and Turing–Hopf patterning of the disease. *Phys. A: Stat. Mech. its Appl.* **545**, 123773 (2020).
20. M Banerjee, V Volpert, P Manfredi, A D'onofrio, Behavior-induced phase transitions with far from equilibrium patterning in a SIS epidemic model: Global vs non-local feedback. *Phys. D: Nonlinear Phenom.* **469**, 134316 (2024).
21. M Banerjee, S Ghosh, P Manfredi, A d'Onofrio, Spatio-temporal chaos and clustering induced by nonlocal information and vaccine hesitancy in the SIR epidemic model. *Chaos, Solitons & Fractals* **170**, 113339 (2023).
22. Z He, P Manfredi, A d'Onofrio, CT Bauch, Homophily in a multi-group vaccination game and its impact on disease dynamics. *Proc. Royal Soc. B: Biol. Sci.* **293** (2026).
23. Z Tai, T Sun, Media dependencies in a changing media environment: The case of the 2003 SARS epidemic in China. *New Media & Soc.* **9**, 987–1009 (2007).
24. Q Liu, et al., Health communication through news media during the early stage of the COVID-19 outbreak in China: digital topic modeling approach. *J. Med. Internet Res.* **22**, e19118 (2020).
25. World Health Organization. 2020 Feb 21. Coronavirus disease 2019 (COVID-19) situation report – 32 (https://www.who.int/docs/default-source/coronaviruse/situation-reports/20200221-sitrep-32-covid-19.pdf?sfvrsn=4802d089_2) (2020) Accessed: 2025-08-26.
26. T Oshio, H Kimura, T Nishizaki, S Kuwahara, At which area level does COVID-19 infection matter most for an individual's self-rated health? A multilevel fixed-effects model analysis in Japan. *Int. J. Environ. Res. Public Heal.* **19**, 8918 (2022).
27. NB Schmidt, et al., Actual versus perceived infection rates of COVID-19: Impact on distress, behavior and disability. *J. Psychiatr. Res.* **137**, 525–533 (2021).
28. S Li, Z Zhang, Y Liu, S Ng, The closer I am, the safer I feel: The "distance proximity effect" of COVID-19 pandemic on individuals' risk assessment and irrational consumption. *Psychol. & Mark.* **38**, 2006–2018 (2021).
29. S Öner, K Szpunar, LA Watson, S Cole, Spatial optimism in individuals' future thinking about the COVID-19 pandemic. *Appl. Cogn. Psychol.* **39**, e70080 (2025).
30. JD Murray, JD Murray, *Mathematical Biology: I. An Introduction.* (Springer), (2002).
31. A Lajmanovich, JA Yorke, A deterministic model for gonorrhea in a nonhomogeneous population. *Math. Biosci.* **28**, 221–236 (1976).
32. WI Hyun, YH Son, SO Jung, Infection preventive behaviors and its association with perceived threat and perceived social factors during the covid-19 pandemic in south korea: 2020 community health survey. *BMC Public Heal.* **22**, 1381 (2022).
33. PE Smaldino, LM Aplin, DR Farine, Sigmoidal acquisition curves are good indicators of conformist transmission. *Sci. Reports* **8**, 14015 (2018).
34. J Guckenheimer, P Holmes, *Nonlinear Oscillations, Dynamical Systems, and Bifurcations of Vector Fields.* (Springer Science & Business Media) Vol. 42, (2013).
35. M Golubitsky, DG Schaeffer, *Singularities and Groups in Bifurcation Theory: Volume I.* (Springer Science & Business Media), pp. 6–10 (1985).
36. AS Bizyaeva, "Nonlinear dynamics of multi-agent multi-option belief and opinion formation," PhD thesis, Princeton University (2022).
37. WR Inc., Mathematica, Version 14.3 (2025).
38. A Dhooge, W Govaerts, YA Kuznetsov, MATCONT: a MATLAB package for numerical bifurcation analysis of ODEs. *ACM Transactions on Math. Softw. (TOMS)* **29**, 141–164 (2003).
39. TM Inc., MATLAB, Version 23.2.0 (R2023b) (2023).
40. O Diekmann, JAP Heesterbeek, JAJ Metz, On the definition and the computation of the basic reproduction ratio R_0 in models for infectious diseases in heterogeneous populations. *J. Math. Biol.* **28**, 365–382 (1990).
41. E Kondilis, D Papamichail, V Gallo, A Benos, COVID-19 data gaps and lack of transparency undermine pandemic response. *J. Public Heal.* **43**, e307–e308 (2021).
42. SWX Ong, BE Young, DC Lye, Lack of detail in population-level data impedes analysis of SARS-CoV-2 variants of concern and clinical outcomes. *The Lancet Infect. Dis.* **21**, 1195–1197 (2021).
43. CC Ezeibe, et al., Political distrust and the spread of COVID-19 in Nigeria. *Glob. Public Heal.* **15**, 1753–1766 (2020).
44. Q Yan, et al., Impact of media reports on the early spread of COVID-19 epidemic. *J. Theor. Biol.* **502**, 110385 (2020).
45. DC Glik, Risk communication for public health emergencies. *Annu. Rev. Public Heal.* **28**, 33–54 (2007).
46. ML Holshue, et al., First case of 2019 novel coronavirus in the United States. *New Engl. J. Medicine* **382**, 929–936 (2020).
47. M Alexander, L Unruh, A Koval, W Belanger, United States response to the COVID-19 pandemic, January–November 2020. *Heal. Econ. Policy Law* **17**, 62–75 (2022).
48. A Schuchat, Public health response to the initiation and spread of pandemic COVID-19 in the United States, February 24–April 21, 2020. *Morb. Mortal. Wkly. Rep.* **69** (2020).
49. V Balakrishnan, WZ Ng, MC Soo, GJ Han, CJ Lee, Infodemic and fake news–A comprehensive overview of its global magnitude during the COVID-19 pandemic in 2021: A scoping review. *Int. J. Disaster Risk Reduct.* **78**, 103144 (2022).
50. V Suarez-Lledo, J Alvarez-Galvez, Prevalence of health misinformation on social media: systematic review. *J. Med. Internet Res.* **23**, e17187 (2021).
51. S Gerdes, M Rank, I Glauche, I Roeder, Impact of exposure frequency on disease burden of the common cold–a mathematical modeling perspective. *PLoS One* **20**, e0334527 (2025).
52. MS Mahmud, S Eshun, B Espinoza, C Kadelka, Adaptive human behavior and delays in information availability autonomously modulate epidemic waves. *PNAS Nexus* **4**, pgaf145 (2025).
53. A Atalan, Is the lockdown important to prevent the covid-19 pandemic? effects on psychology, environment and economy-perspective. *Annals medicine surgery* **56**, 38–42 (2020).
54. W Yamaka, S Lomwanawong, D Magel, P Maneejuk, Analysis of the lockdown effects on the economy, environment, and covid-19 spread: lesson learnt from a global pandemic in 2020. *Int. journal environmental research public health* **19**, 12868 (2022).
55. E Bendavid, C Oh, J Bhattacharya, JP Ioannidis, Assessing mandatory stay-at-home and business closure effects on the spread of COVID-19. *Eur. J. Clin. Investig.* **51**, e13484 (2021).
56. CM Saad-Roy, A Traulsen, Dynamics in a behavioral–epidemiological model for individual adherence to a nonpharmaceutical intervention. *Proc. Natl. Acad. Sci.* **120**, e2311584120 (2023).

Supporting Information for

Attention to heterogeneous information sources affects epidemic outcomes

Jiayu Li, Matthew Cheung, Marcela Ordorica Arango, Naomi Ehrich Leonard and Simon A. Levin

Jiayu Li, Naomi Ehrich Leonard, Simon A. Levin
E-mail: jl2894@princeton.edu, naomi@princeton.edu, slevin@princeton.edu

This PDF file includes:

Supporting Information Text

Derivation of the model. Here, we present the derivation of dynamics of the perceived infection.

Consider a small change in time Δt, we have $p_{s1}(t+\Delta t) = p_{s1}(t) + \Delta t(\eta_1 p_1(t+\Delta t) + (1-\eta_1)p_2(t+\Delta t) - p_{s1}(t))$, where $\eta_1 p_1(t+\Delta t) + (1-\eta_1)p_2(t+\Delta t)$ is the perceived infection at time $t+\Delta t$, and $p_{s1}(t)$ is the perceived infection at time t, which is outdated. We then have $\frac{p_{s1}(t+\Delta t)-p_{s1}(t)}{\Delta t} = \eta_1 p_1(t+\Delta t) + (1-\eta_1)p_2(t+\Delta t) - p_{s1}(t)$. Taking $\Delta t \to 0$, we get the dynamics of p_{s1}. A similar derivation works for p_{s2}.

Bifurcation from IFE to UEE. The Jacobian $J(p_1, p_2, p_{s1}, p_{s2})$ of the system of equations comprising the mathematical model is computed to be

$$\begin{pmatrix} \beta\alpha(p_{s1})(k-2kp_1-(1-k)p_2)-1 & \beta\alpha(p_{s1})(1-p_1)(1-k) & \beta\alpha'(p_{s1})(1-p_1)(kp_1+(1-k)p_1) & 0 \\ \beta\alpha(p_{s2})(1-p_2)(1-k) & \beta\alpha(p_{s2})(k-2kp_2-(1-k)p_1)-1 & 0 & \beta\alpha'(p_{s2})(1-p_2)(kp_2+(1-k)p_1) \\ \frac{\eta_1}{\tau} & \frac{1-\eta_1}{\tau} & -\frac{1}{\tau} & 0 \\ \frac{1-\eta_2}{\tau} & \frac{\eta_2}{\tau} & 0 & -\frac{1}{\tau} \end{pmatrix}.$$

At the IFE, where $p_1 = p_2 = p_{s1} = p_{s2} = 0$, and recalling that $\alpha(0) = 1$, the Jacobian reduces to

$$J(0,0,0,0) = \begin{pmatrix} k\beta-1 & (1-k)\beta & 0 & 0 \\ (1-k)\beta & k\beta-1 & 0 & 0 \\ \frac{\eta_1}{\tau} & \frac{1-\eta_1}{\tau} & -\frac{1}{\tau} & 0 \\ \frac{1-\eta_2}{\tau} & \frac{\eta_2}{\tau} & 0 & -\frac{1}{\tau} \end{pmatrix},$$

which has eigenvalues $\beta-1$, $(2k-1)\beta-1$ and $-\frac{1}{\tau}$. We know that $2k-1 \le 1$ since $k \in [0,1]$. So for $k<1$, the eigenvalue $\beta-1$ is simple and dominant. If $\beta > 1 = \beta^*$, the first eigenvalue is positive and so the IFE loses stability. This threshold does not depend on other parameter values.

The IFE at $\beta = \beta^* = 1$ is a singularity since $J(0,0,0,0;\beta=\beta^*)$ has a zero eigenvalue. We perform the Lyapunov-Schmidt reduction (1) of the dynamics about the IFE and $\beta = \beta^*$ to prove that the singularity corresponds to a bifurcation and to derive the local bifurcation diagram. The right eigenvector $\mathbf{v}$ and left eigenvector $\mathbf{w}$ corresponding to the zero eigenvalue of $J(0,0,0,0;\beta=\beta^*)$ are $\mathbf{v} = \begin{pmatrix}1\\1\\1\\1\end{pmatrix}$, $\mathbf{w} = \begin{pmatrix}1\\1\\0\\0\end{pmatrix}$.

Following the procedure in (2), the Lyapunov Schmidt reduction gives us a scalar equation for the local bifurcation diagram: $f(p,\gamma) = c_1\gamma + c_2\gamma p + c_3 p^2 + c_4 p^3 + h.o.t. = 0$, where scalar p is the restriction of $(p_1, p_2, p_{s1}, p_{s2})$ to $\mathbf{v}$ and $\gamma = \beta - \beta^*$. The coefficients are $c_1 = 0$, $c_2 = 2$, $c_3 = -4\beta^* + 4\beta^*\alpha'(0)$.

This reduction, along the direction of $\mathbf{v}$, can be shown to be isomorphic to the normal form of a transcritical bifurcation if $c_2 \neq 0$ and $c_3 < 0$, which is always true since $\alpha'(0) < 0$.

When $k = 1$, the reduction will be a projection onto a two-dimensional space, which is more complicated. However, numerically, the transition from IFE to UEE is observed (Fig. S1).

Implication of the stability of UEE. At the UEE, we have $p_1 = p_2 = p_{s1} = p_{s2} = p$, where p satisfies

$$\beta\alpha(p)(1-p) = 1. \qquad [1]$$

Note that p exists and is unique as both $\alpha(\cdot)$ and $1-p$ are decreasing for $p \in [0,1]$. The corresponding Jacobian at the UEE is

$$J(p,p,p,p) = \begin{pmatrix} \beta\alpha(p)(k-kp-p)-1 & 1-k & \beta\alpha'(p)(1-p)p & 0 \\ 1-k & \beta\alpha(p)(k-kp-p)-1 & 0 & \beta\alpha'(p)(1-p)p \\ \frac{\eta_1}{\tau} & \frac{1-\eta_1}{\tau} & -\frac{1}{\tau} & 0 \\ \frac{1-\eta_2}{\tau} & \frac{\eta_2}{\tau} & 0 & -\frac{1}{\tau} \end{pmatrix}$$

with eigenvalues $\frac{(1-\beta\alpha(p))\tau-1 \pm \sqrt{[(1-\beta\alpha(p))\tau-1]^2+4\tau(\beta\alpha'(p)(1-p)p-\beta\alpha(p)p)}}{2\tau}$ and $\frac{\tau(2k-\beta\alpha(p)-1)-1 \pm \sqrt{[\tau(2k-\beta\alpha(p)-1)-1]^2+4\tau(2k-\beta\alpha(p)+(\eta_1+\eta_2-1)\beta\alpha'(p)p(1-p)-1)}}{2\tau}$.

The first pair of eigenvalues always has negative real part given $\alpha'(p) < 0$. For the second pair of eigenvalues, we first note that $\tau(2k-\beta\alpha(p)-1)-1 \le \tau(1-\beta\alpha(p))-1 = \tau(\beta\alpha(p)(1-p)-\beta\alpha(p))-1 = -\tau\beta\alpha(p)p - 1 < 0$. Suppose $[\tau(2k-\beta\alpha(p)-1)-1]^2 + 4\tau(2k-\beta\alpha(p)+(\eta_1+\eta_2-1)\beta\alpha'(p)p(1-p)-1) < 0$, the real part of the pair of eigenvalues stays negative, thus we only need to consider the case when $[\tau(2k-\beta\alpha(p)-1)-1]^2+4\tau(2k-\beta\alpha(p)+(\eta_1+\eta_2-1)\beta\alpha'(p)p(1-p)-1) \ge 0$, when the pair of eigenvalues are purely real. It turns out that when $4\tau(2k-\beta\alpha(p)+(\eta_1+\eta_2-1)\beta\alpha'(p)p(1-p)-1) < 0$, the largest real part of the eigenvalues stays negative. Consequently, the UEE stays stable if

$$\eta_1 + \eta_2 > \frac{1-2k+\beta\alpha(p)}{\beta\alpha'(p)p(1-p)} + 1 = C_0. \qquad [2]$$

Note here C_0 does not depend on the value of $\tau > 0$. Since $\alpha'(\cdot) < 0$ and $1-2k+\beta\alpha(p) > 0$, we have $C_0 < 1$.

We note that the value of β also affects the stability of the UEE. In particular, the critical value of β at which point the UEE loses stability is always strictly greater than 1, see Fig. S2.

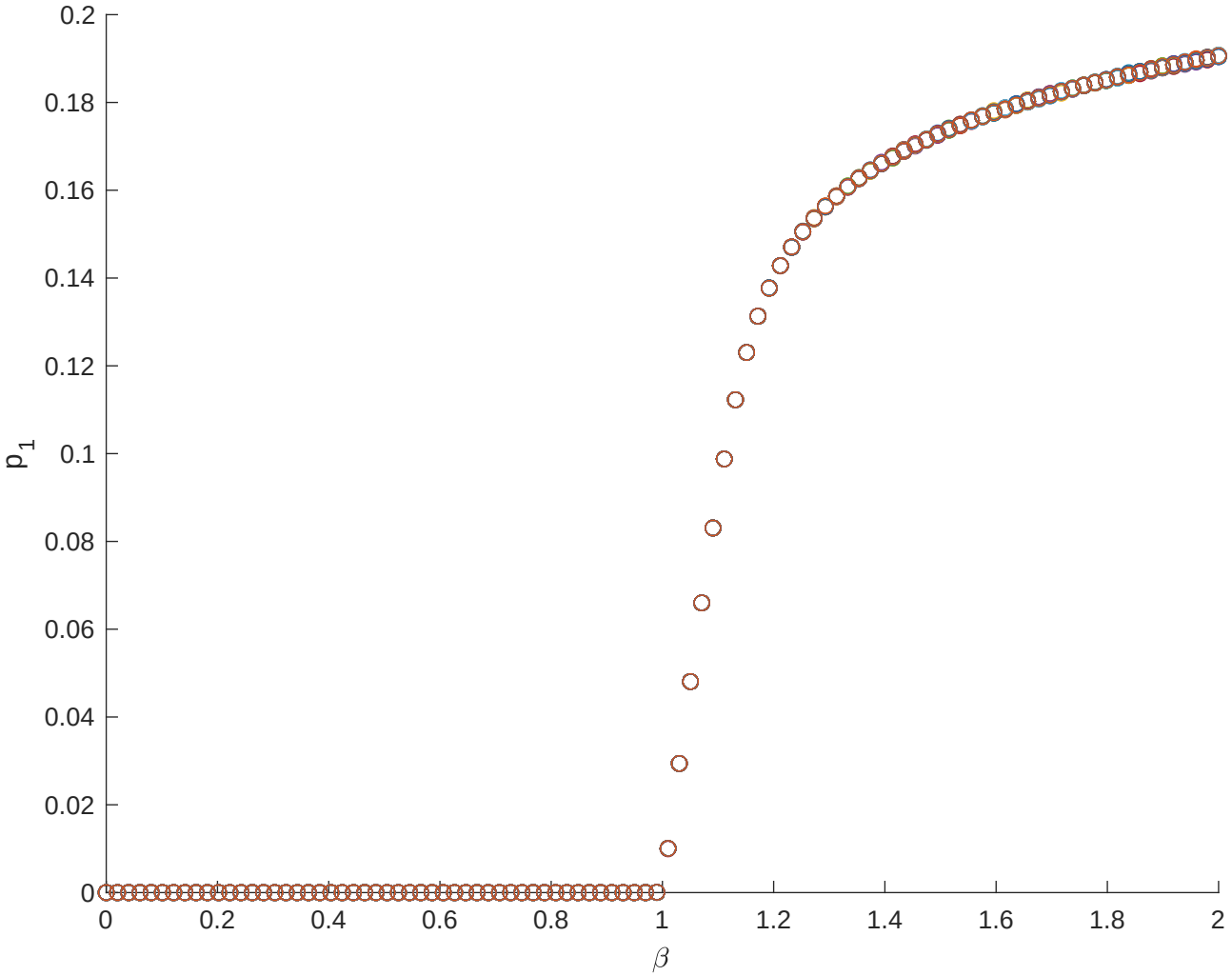

Fig. S1. Equilibrium p_1 when $k = 1$, $\eta_1 = \eta_2 = 0.9$, $\mu = 0.2$, $\nu = 8$. For each value of β, 100 random initial conditions are chosen and the simulations are run. When $\beta < \beta^* = 1$, all equilibria p_1 are IFE, and when $\beta > \beta^* = 1$, all equilibria p_1 are at a UEE.

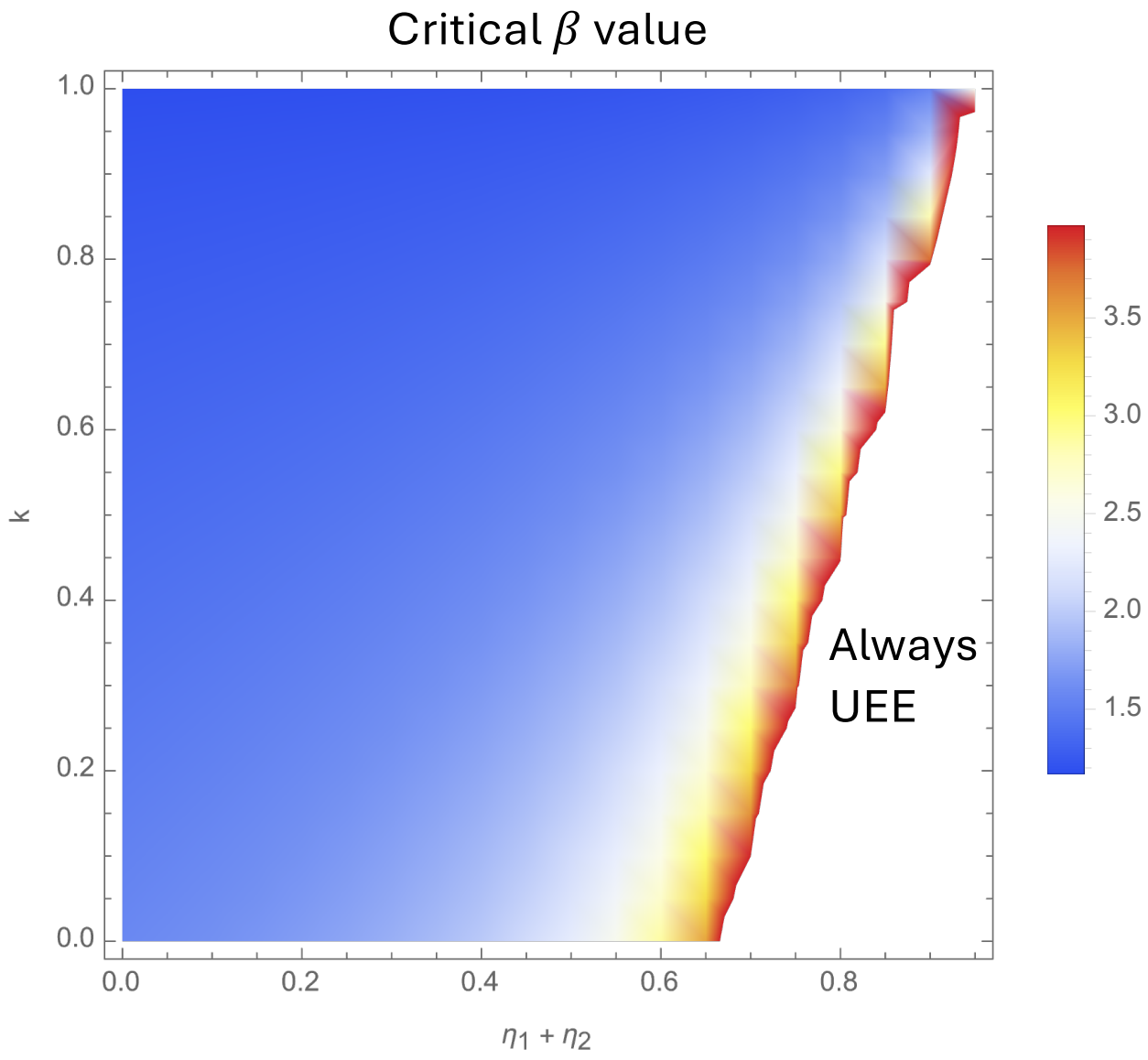

Fig. S2. The critical value of β when the UEE loses stability. $\mu = 0.2$, $\nu = 8$. The minimum possible value ($\beta = 1.17$) occurs at $k = 1$, $\eta_1 + \eta_2 = 0$.

Bifurcation from UEE to NUEE. The proof is presented for $k = 1$. The argument is similar for other values of k, and the bifurcation can be observed numerically when UEE becomes unstable, see Fig. S3. However, the analytical expression for the coefficients of the reduction is hard to obtain, as it involves calculating the inverse of a symbolic matrix.

Let η_1 be the bifurcation parameter. As discussed above, the UEE $p_1 = p_2 = p_3 = p_4 = p^*$ at $\eta_1 = \eta^*$ is a singularity when $\eta^* = C_0 - \eta_2$, since $J(p^*, p^*, p^*, p^*; \eta_1 = \eta^*)$ has a zero eigenvalue. Note that with Eq. **1**, p^* and η^* can be found explicitly (or at least numerically). We perform the Lyapunov-Schmidt reduction (1) of the dynamics about the the UEE at $\eta_1 = \eta^*$ to prove that the singularity corresponds to a local bifurcation and to derive the local bifurcation diagram.

Denote $A = \beta\alpha(p^*)(1-2p^*) - 1, B = \beta\alpha'(p^*)(1-p^*)p^*$, $E = \frac{1}{\eta^*+\eta_2-1}$, and $F = -\frac{1-\eta^*}{1-\eta_2}$. The right eigenvector $\mathbf{v}$ and left eigenvector $\mathbf{w}$ corresponding to the zero eigenvalue of $J(p^*, p^*, p^*, p^*; \eta_1 = \eta^*)$ are $\mathbf{v} = \begin{pmatrix} -\frac{1-\eta^*}{(1-\eta_2)(\eta^*+\eta_2-1)} \\ \frac{1}{\eta^*+\eta_2-1} \\ -\frac{1-\eta^*}{1-\eta_2} \\ 1 \end{pmatrix}$, $\mathbf{w} = \begin{pmatrix} -\frac{1}{\tau B} \\ \frac{1}{\tau B} \\ -1 \\ 1 \end{pmatrix}$.

Since $\eta^* + \eta_2 - 1 < 0$ and $\eta^*, \eta_2 \geq 0$, $\mathbf{v}$ is properly defined.

Define the vector $\mathbf{x}$ with components $x_1 = p_1 - p^*$, $x_2 = p_2 - p^*$, $x_3 = p_{s1} - p^*$, $x_3 = p_{s1} - p^*$, $x_4 = p_{s2} - p^*$ and let $\gamma = \eta_1 - \eta^*$. Writing the system dynamics in these coordinates, the origin $\mathbf{x} = \mathbf{0}$ at $\gamma = 0$ is a singularity:

$$\begin{aligned}
\frac{dx_1}{dt} &= \beta\alpha(x_3 + p^*)(1 - x_1 - p^*)(x_1 + p^*) - x_1 - p^* \\
\frac{dc_2}{dt} &= \beta\alpha(x_4 + p^*)(1 - x_2 - p^*)(x_2 + p^*) - x_2 - p^* \\
\tau\frac{dx_3}{dt} &= -x_3 - p^* + (\gamma + \eta^*)(x_1 + p^*) + (1 - \gamma - \eta^*)(x_2 + p^*) \\
\tau\frac{dx_4}{dt} &= -x_4 - p^* + \eta_2(x_2 + p^*) + (1 - \eta_2)(x_1 + p^*).
\end{aligned}$$

The Lyapunov Schmidt reduction gives us a scalar equation for the bifurcation diagram: $f(x, \gamma) = c_1\gamma + c_2\gamma x + c_3x^2 + c_4x^3 + h.o.t = 0$, where the scalar x is $\mathbf{x}$ restricted to $\mathbf{v}$. We have $c_1 = 0$, $c_3 = \frac{1-F^2}{\tau B}(-2\beta\alpha(p^*)E^2 + 2\beta\alpha'(p^*)(1-2p^*)E + \beta\alpha''(p^*)(1-p^*)p^*)$, and $c_2 = \frac{1}{\tau}E(1-F) \neq 0$. Here, the signs of c_2 and c_3 do not depend on the value of τ, given $\tau > 0$.

From this we can show that if $\eta^* \neq \eta_2$, $c_3 \neq 0$, a transcritical bifurcation happens locally. Through numerical simulation we observe that $c_4 \neq 0$ (Fig. S3). Following (1, 3), the system contains an unfolding of a pitchfork bifurcation where c_3 is the unfolding parameter. When $c_3 = 0$, the reduction is isomorphic to the normal form of a pitchfork bifurcation. When $c_3 \neq 0$, the pitchfork unfolds and a transcritical bifurcation happens locally, with an additional saddle node bifurcation. The signs of c_2 and c_4 determine the direction of the bifurcation.

Effect of τ. Although, for the parameter regime studied, τ does not affect the values and stability of the equilibria (including IFE, UEE and NUEE), nor the type of local bifurcations that result in transitions among those three equilibria, it does affect the transient dynamics of the system. In particular, as τ increases, i.e., the dynamics of the perceived infection become slower compared to the dynamics of the disease transmission, it takes more time for the system to reach the NUEE equilibrium and there is more oscillatory behavior in the transient dynamic. For τ large enough, the oscillation during the transient dynamics is so strong that it is possible that the infection levels in both groups become very low before they bounce back to reach the endemic equilibrium, see Fig. S4. Given that we focus on the local analysis near the bifurcation point, it can be interesting in future work to investigate the more global effects of τ.

Instantaneous perception update. In this subsection, we consider the special case where the perceived infection update is instantaneous, i.e. $\tau \to 0$, which allows us to reduce the 4-dimensional system to a 2-dimensional system:

$$\begin{aligned}
\frac{dp_1}{dt} &= \beta\alpha(\eta_1p_1 + (1-\eta_1)p_2)(kp_1 + (1-k)p_2))(1-p_1) - \delta p_1 \\
\frac{dp_2}{dt} &= \beta\alpha(\eta_2p_2 + (1-\eta_2)p_1)(kp_2 + (1-k)p_1))(1-p_2) - \delta p_2.
\end{aligned}$$

We mainly consider the stabilty of UEE (where $p_1 = p_2 = p$) in this subsection. With some algebra, we find the corresponding Jacobian at the UEE to be

$$J(p,p) = \begin{pmatrix} \beta\alpha'(p)\eta_1p(1-p) + k - \beta\alpha(p) & \beta\alpha'(p)(1-\eta_1)p(1-p) + 1 - k \\ \beta\alpha'(p)(1-\eta_2)p(1-p) + 1 - k & \beta\alpha'(p)\eta_2p(1-p) + k - \beta\alpha(p) \end{pmatrix}.$$

For the UEE to be stable, we want $Tr(J(p,p)) < 0$ and $Det(J(p,p)) > 0$. This gives us the condition $\eta_1 + \eta_2 > \frac{1-2k+\beta\alpha(p)}{\beta\alpha'(p)p(1-p)} + 1$, which confirms the stability condition we have in the 4-dimensional system.

Lyapunov Schmidt reduction for this system, again, gives us a scalar equation for the local bifurcation diagram. Suppose at $p = p^*, \eta_1 = \eta^*$, the UEE loses stability. Let

$$J(p^*, p^*) = \begin{pmatrix} A & B \\ C & D \end{pmatrix}.$$

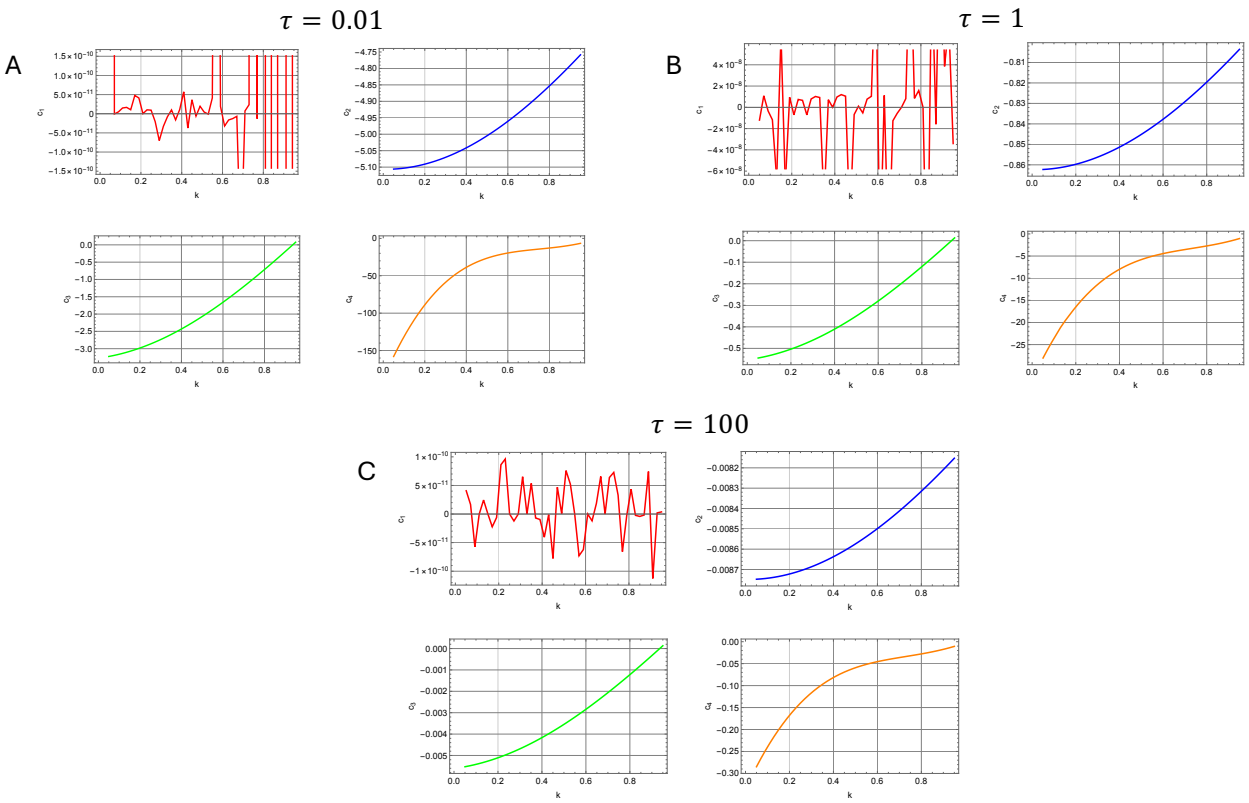

Fig. S3. Numerical computation of the coefficients of the Lyapunov Schmidt reduction of the system for different values of k when $\eta_2 = 0.1$ (Here we choose $\eta_2 < C_0$ for $\forall k \in [0, 1]$, so the bifurcation will happen as k change.) Different subplots have different τ. Across three subplots, same trend in the sign of the coefficients are observed. c_1 is very close to 0. c_2 and c_4 are always negative, c_3 is negative for small k, and becomes positive for large k. The exact values don't matter due to non-uniqueness of eigenvectors.

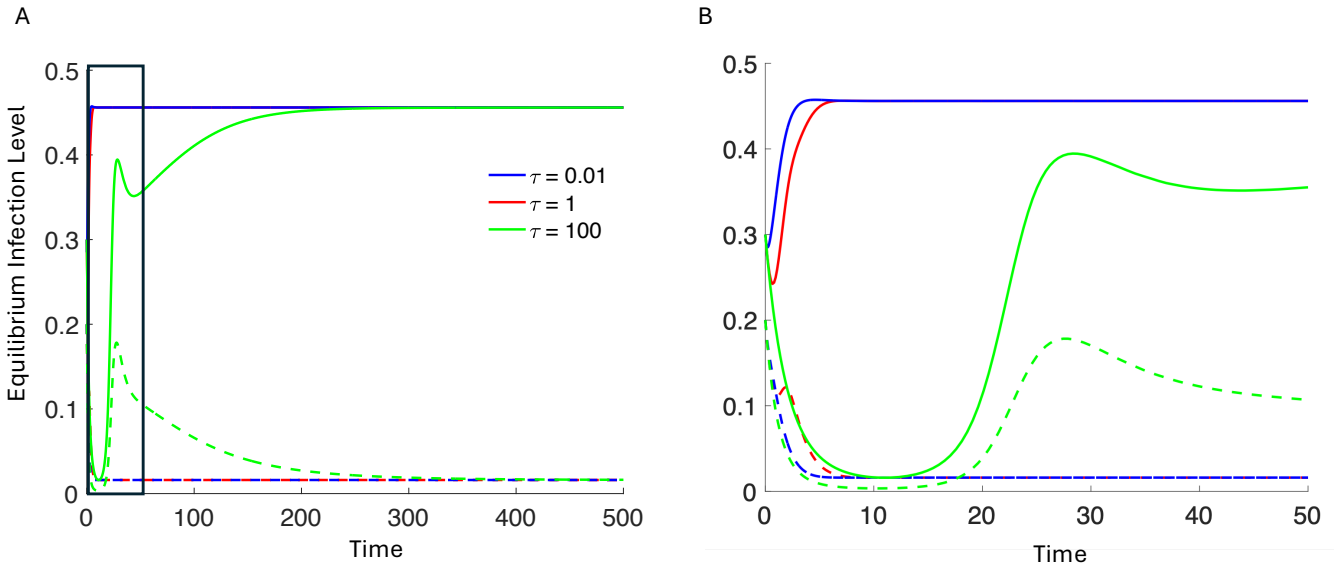

Fig. S4. Dynamics of the system with different values of τ when NUEE is stable. Panel B is the enlarged version of the box in Panel A, which provides better representation of the transient dynamics. Solid line represents $p_1(t)$, dashed line represents $p_2(t)$, $p_1(0) = 0.3, p_2(0) = 0.2, \beta = 3, k = 0.6, \eta_1 = 0.2, \eta_2 = 0.4$.

where $A = \eta_1\beta\alpha'(p^*)p^*(1-p^*)+k-\beta\alpha(p^*)$, $B = (1-\eta_1)\beta\alpha'(p^*)p^*(1-p^*)+1-k$, $C = (1-\eta_2)\beta\alpha'(p^*)p^*(1-p^*)+1-k$, $D = \eta_2\beta\alpha'(p^*)p^*(1-p^*)+k-\beta\alpha(p^*)$.

After some algebra, we have $c_1 = 0$, $c_2 = \beta\alpha'(p^*)p^*(1-p^*)\frac{D}{B}(1+\frac{D}{C}) \neq 0$, and $c_3 = \beta\alpha''(p^*)p^*(1-p^*)(-\frac{D^3}{BC^2}\eta^{*2}+\frac{D^2}{BC}\eta^*(1-\eta^*)-\frac{D}{B}(1-\eta^*)^2+\eta_2^2-\frac{D}{C}\eta_2(1-\eta_2)+\frac{D^2}{C^2}(1-\eta_2)^2)+\beta\alpha'(p^*)(k-kp^*-p^*)(-\frac{2D^3}{BC^2}\eta^*+\frac{D^2}{BC}(1-\eta^*)+2\eta_2-\frac{D}{C}(1-\eta_2))+\beta\alpha'(p^*)(1-k)(1-p^*)(\frac{D^2}{BC}\eta^*-\frac{2D}{B}(1-\eta^*)-\frac{D}{C}\eta_2+\frac{2D^2}{C^2}(1-\eta_2))+\beta\alpha(p^*)(\frac{2D^3}{BC^2}k-(1-k)\frac{D^2}{BC}-2k+\frac{D}{C}(1-k))$

The coefficients for the reduction are still complicated that it is hard to obtain more analytical insights for this reduced system. However, numerically, the same bifurcation in 4-dimensional system is observed in this reduced 2-dimensional system, see Fig. S5. We retain the dynamics of the perceived infection (i.e., keep τ positive) in any case because it is not so practical to assume that people instantaneously update their perception of disease, and positive τ relates to a more general case for the update of perceived infection.

Effect of initial infection level on equilibrium infection level. It is necessary that $\eta_1+\eta_2<1$ for the UEE to be unstable, which then implies $p_{s1}(0) \geq p_{s2}(0)$ if $p_1(0) \leq p_2(0)$, by our assumption of initial conditions in Eq. **2** of the main text. With this implicit assumption, the proof is as follow.

Define $u = p_1 - p_2$, $v = p_{s1} - p_{s2}$. We want to show that the region where $u \leq 0, v \geq 0$ is positively invariant. To check this, we need to check the boundary of the region.

First, let $u = 0$, i.e., $p_1 = p_2 = p$. Then $\dot{u}|_{u=0} = \beta(\alpha(p_{s1}) - \alpha(p_{s2}))p(1-p)$. Suppose $v \geq 0$, i.e., $p_{s1} \geq p_{s2}$. Since $\alpha(\cdot)$ is a decreasing function, we have $\dot{u}|_{u=0} \leq 0$. Then, let $v = 0$. Then, $\dot{v} = -v - (1-\eta_1-\eta_2)u$ and $\dot{v}|_{v=0} = -(1-\eta_1-\eta_2)u$. For $u \leq 0$, we have $\dot{v}|_{v=0} \geq 0$. Consequently, the region $u \leq 0, v \geq 0$ is positively invariant, which completes the proof.

A symmetric argument works to prove the case when $p_1(0) > p_2(0)$.

General Case of SIRS. We show numerically that key conclusions stated in the main text hold if the disease transmission follows the more general SIRS dynamicsin the case that the rate of waning immunity is sufficiently high. These results include the transcritical bifurcation with respect to the information choice and the optimal informational strategy for one group, and for the whole population.

Using a similar modeling approach as in the case of SIS in the main text, the SIRS disease model coupled with the spread of awareness of disease has the form:

$$\begin{aligned}
\frac{dp_1}{dt} &= \beta\alpha(p_{s1})(kp_1+(1-k)p_2)s_1 - \delta p_1 \\
\frac{dp_2}{dt} &= \beta\alpha(p_{s2})(kp_2+(1-k)p_1)s_2 - \delta p_2 \\
\tau\frac{dp_{s1}}{dt} &= -p_{s1} + \eta_1 p_1 + (1-\eta_1)p_2 \\
\tau\frac{dp_{s2}}{dt} &= -p_{s2} + \eta_2 p_2 + (1-\eta_2)p_1. \\
\frac{ds_1}{dt} &= -\beta\alpha(p_{s1})(kp_1+(1-k)p_2)s_1 + \sigma(1-s_1-p_1) \\
\frac{ds_2}{dt} &= -\beta\alpha(p_{s2})(kp_2+(1-k)p_1)s_2 + \sigma(1-s_2-p_2).
\end{aligned}$$

As before, p_i and p_{si} represents the actual and perceived infection of group i, s_i is the proportion of susceptible individuals in group i. With rate β, susceptible individuals are infected by infected individuals, and with rate δ, infected individuals become recovered individuals, where they get immunity towards infection. As the immunity wanes with rate σ, the recovered individuals becomes susceptible again.

While the analytical proofs we provided for the SIS model are not so easy to apply to this SIRS model , we can show numerically that the bifurcation from UEE to NUEE is still observed, see Fig. S6A. However, for σ not so large, i.e., if the immunity wanes slowly, the bifurcation does not happen (Fig. S6B). Intuitively, this connects well to our result in the main text for the SIS model: as σ increases (i.e., recovered individuals lose immunity soon after recovery), the SIRS model behaves more like SIS. For σ large enough, the conclusion still holds that the UEE regime is better for the group that starts with high infection level (Fig. S6C). Additionally, the prosociality result, i.e., that the information source that benefits a group might conflict with the information source that benefits the whole population, still holds for high enough prosociality (Fig. S6D): as for some $\gamma < \frac{1}{2}$, equilibrium $(1-\gamma)p_1 + \gamma p_2$ is minimized in the NUEE region, even though equilibrium p_1 is minimized in the UEE region.

For lower σ, it is harder to observe the bifurcation from UEE to NUEE. As σ decreases, SIRS type models behaves more like SIR and have very low infection levels between waves of infection. Thus it is harder to maintain sustained vigilance of the disease spread.

Although for lower σ the choices of information source do not affect the equilibrium infection levels, we report numerically some transient dynamics that are interesting for future study. Here, we assume $p_1(0) < p_2(0)$, and $\eta_2 = 1$. As η_1 increases, the peak infection level of the first epidemic wave of group 1 increases (Fig. S7B), while the peak infection level of the second epidemic wave does not change significantly (Fig. S7C). The increase in peak infection level of the first epidemic wave with increasing η_1 is consistent with the result for the model studied in this paper, which is that a group is worse off if it focuses its source of information on the group with the lower infection level.

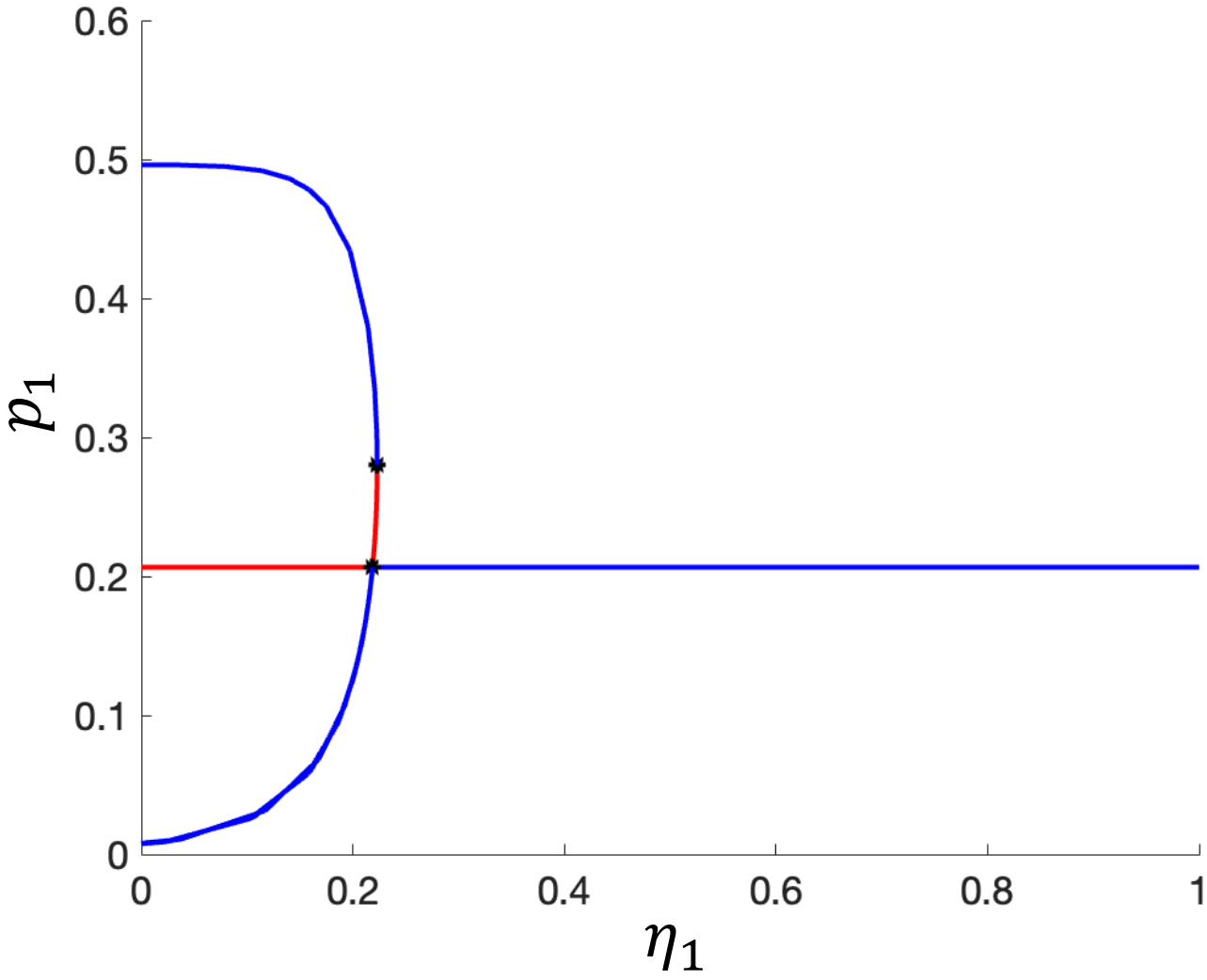

Fig. S5. The reduced 2-dimensional system undergoes an unfolding of a pitchfork bifurcation which locally exhibits as a transcritical bifurcation from UEE to NUEE. The same parameter values to generate Fig. 2B are used here: $\beta = 3$, $k = \eta_2 = 0.6$, $\nu = 8$, $\mu = 0.2$. Numerically, the bifurcation in this figure is the same as the one in Fig. 2B.

We leave for future work the analytical investigation, as well as a more comprehensive study for the transient dynamics of the model with disease transmission following the general SIRS dynamics.

Integration of cost for overestimation. Here, within the framework of this model where there are no dynamics associated with negative consequences of overestimation of risk, we show how a cost associated with overestimation of the risk of disease could affect the optimal information strategy. We look at the equilibrium value of $p_i + c * \max((p_{si} - p_i), 0)$, where c denotes the cost of overestimation. This excludes an explicit cost of underestimation of disease, except for the result that underestimation may lead to higher equilibrium infection levels.

According to Fig. S8, as c increases, i.e., as overestimation of disease risk becomes more costly, the group that starts with lower infection level would seek to leave the NUEE regime, in contrast to when there is no cost for overestimation, where the NUEE regime is optimal. The cost does not affect the group that starts with higher infection level, which always underestimates the risk within the NUEE regime.

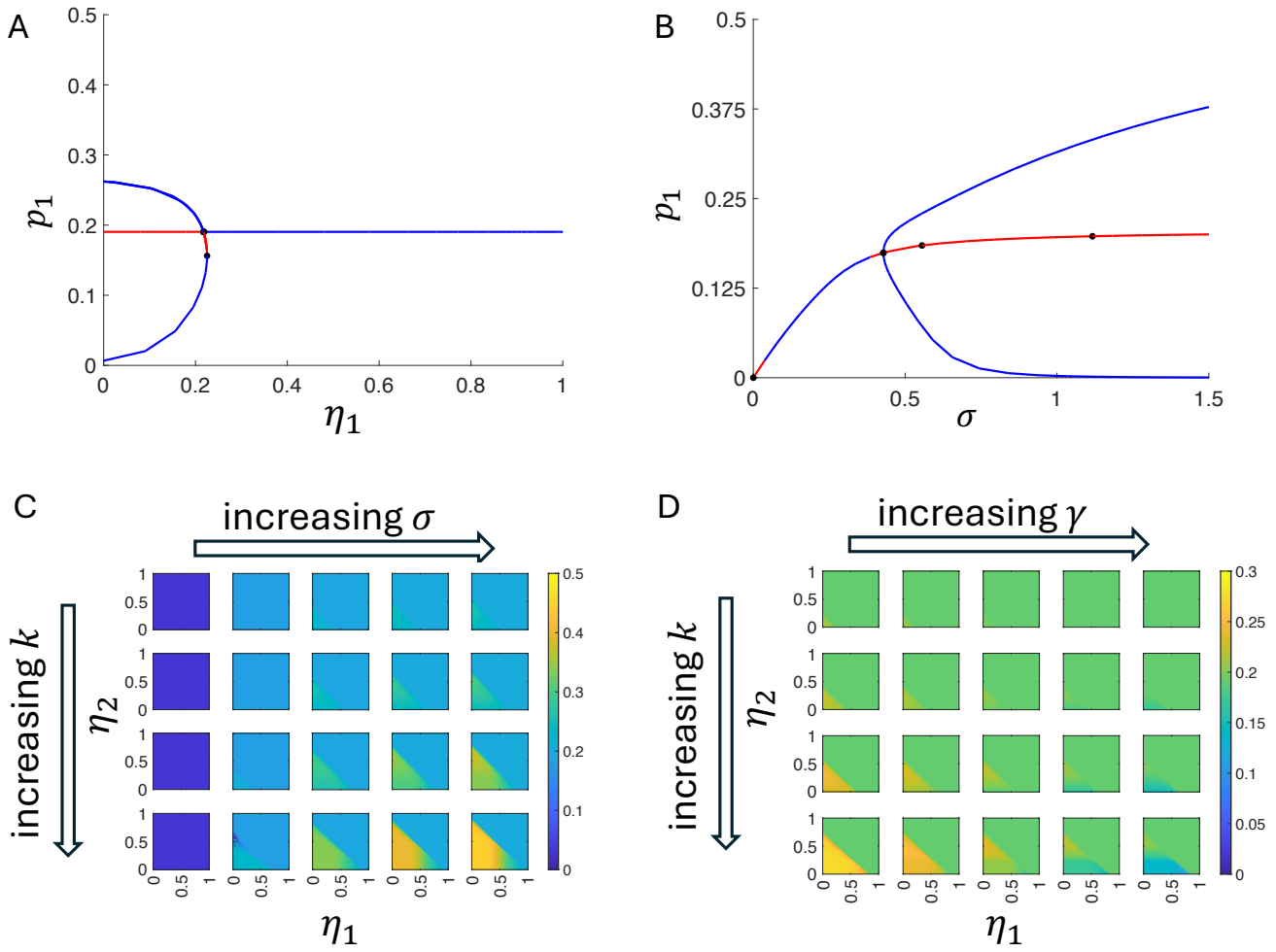

Fig. S6. Bifurcation diagrams for extension to SIRS. Panel A: Bifurcation diagram plots equilibrium value of p_1 as a function of η_1. The system undergoes an unfolding of a pitchfork bifurcation which locally exhibits as a transcritical bifurcation from UEE to NUEE at some critical η_1 value. $\beta = 3$, $\delta = 1$, $\sigma = 0.7$, $k = 0.9$, $\eta_2 = 0.5$, $\tau = 1$. Panel B: Bifurcation diagram plots equilibrium value of p_1 as a function of σ. The system transitions from UEE regime to NUEE regime at some critical σ. $\beta = 3$, $\delta = 1$, $\eta_1 = \eta_2 = 0.1$, $k = 0.9$, $\tau = 1$. Panel C: Equilibrium p_1 in color scale for different k (from 0 to 1) and σ (from 0.05 to 2) values when $p_1(0) > p_2(0)$. β = 3, $\delta = 1$, $\tau = 1$. Panel D: The equilibrium infection level $(1-\gamma)p_1 + \gamma p_2$ in color scale for different values of k (from 0 to 1) and γ (from 0 to $\frac{1}{2}$) in SIRS version of the model when $p_1(0) > p_2(0)$. $\beta = 3$,σ = 0.7, $\delta = 1$, $\tau = 1$.

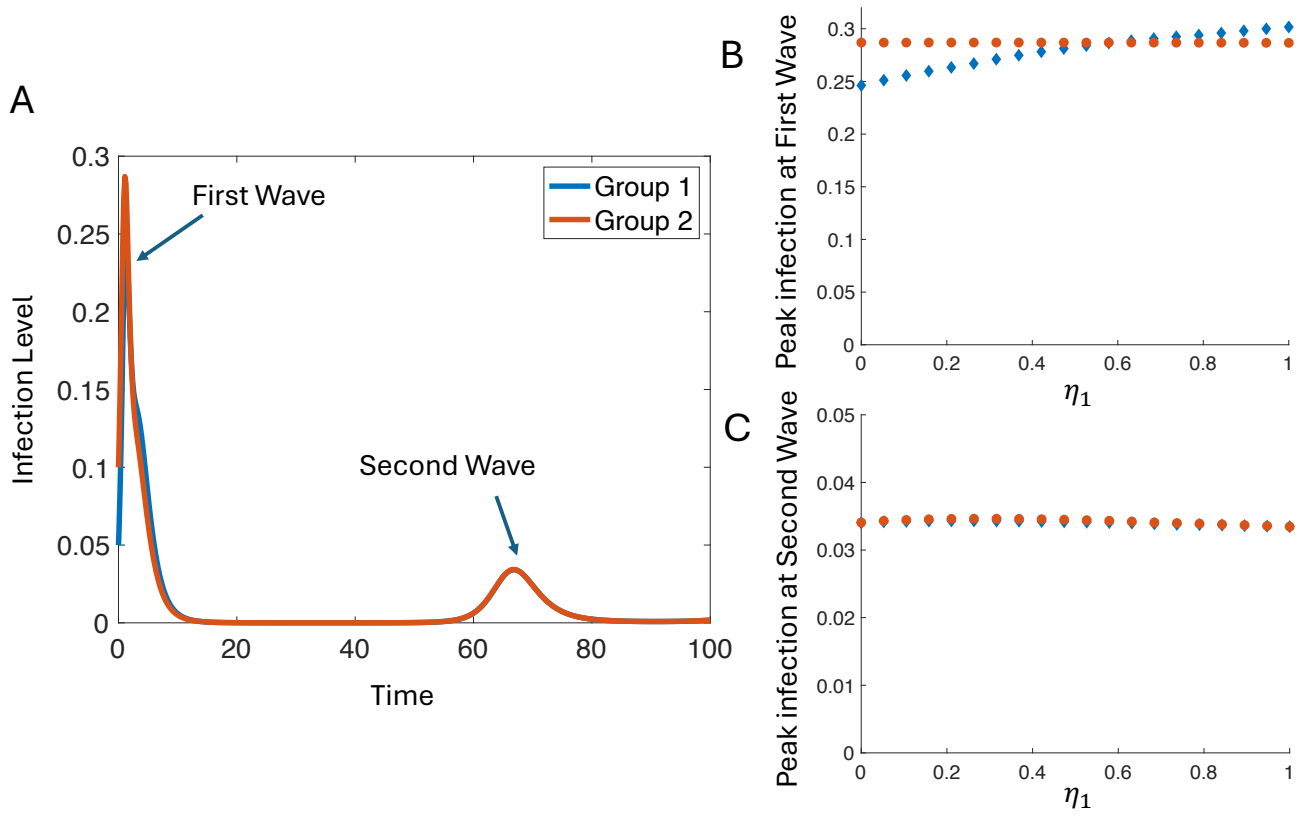

Fig. S7. Transient dynamics of the extension to SIRS for small σ. Panel A: An example of the transient dynamics. $\beta = 3, \gamma = 1, \sigma = 0.01, k = 0.9, \eta_2 = 1, \eta_1 = 0.053, \mu = 0.2, \nu = 8, \tau = 1$. Panel B: The peak infection level of group 1 in the first wave. Panel C: The peak infection level of group 1 in the second wave. $p_1(0) = 0.05, p_2(0) = 0.1$. The exact dynamics may vary depending on the initial conditions, but the general trends hold.

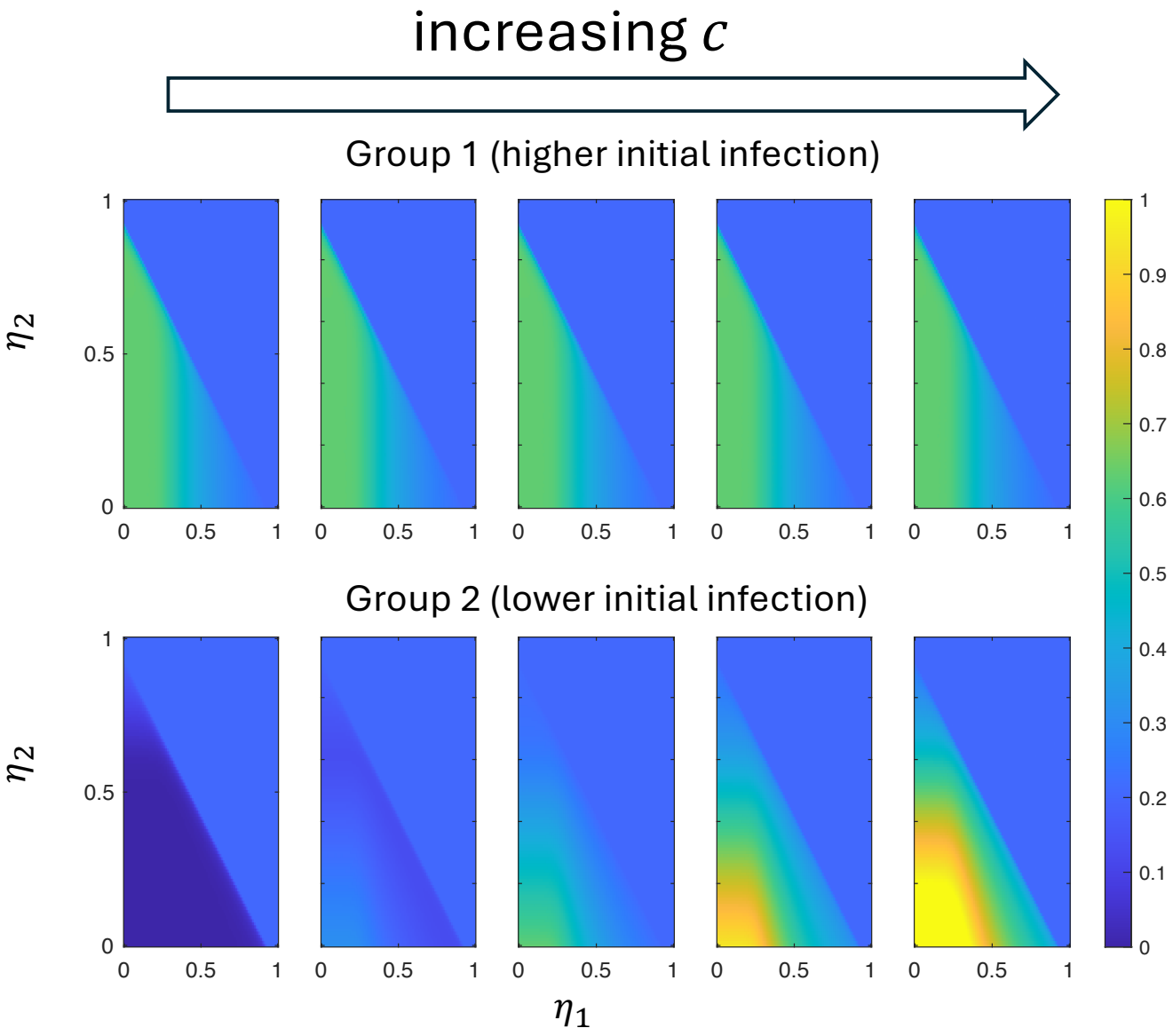

Fig. S8. Illustration of consequences of adding cost for overestimation of the disease risk. Equilibrium $p_i + c * \max(p_{si} - p_i, 0)$ in color scale. $\beta = 3$, $k = 0.9$, c from 0 to 2.

References

1. M Golubitsky, DG Schaeffer, *Singularities and Groups in Bifurcation Theory: Volume I.* (Springer Science & Business Media), pp. 6–10 (1985).
2. AS Bizyaeva, Nonlinear dynamics of multi-agent multi-option belief and opinion formation. Ph.D. thesis (Princeton University) (2022).
3. M Golubitsky, D Schaeffer, A theory for imperfect bifurcation via singularity theory. *Commun. on Pure Appl. Math.* **XXXII**, 21–98 (1979).